Published in final edited form as:

Nature. 2018 May ; 557(7705): 446–451. doi:10.1038/s41586-018-0022-5.

Vms1/Ankzf1 peptidyl-tRNA hydrolase releases nascent chains from stalled ribosomes

Rati Verma[1,2,4], **Kurt M. Reichermeier**[2], **A. Maxwell Burroughs**[3], **Robert S. Oania**[1,2], **Justin M. Reitsma**[2], **L Aravind**[3,*], and **Raymond J. Deshaies**[1,2,4,*]

[1]Howard Hughes Medical Institute, California Institute of Technology, Pasadena, CA 91125 USA

[2]Division of Biology and Biological Engineering, California Institute of Technology, Pasadena, CA 91125 USA

[3]National Center for Biotechnology Information, National Library of Medicine, National Institutes of Health, Bethesda, MD 20894, USA

[4]Amgen, One Amgen Center Way, Thousand Oaks, CA, USA

Ribosomal surveillance pathways scan for ribosomes that are transiently paused or terminally stalled due to structural elements in mRNAs or nascent chain (NC) sequences[1,2]. Some stalls in budding yeast are sensed by the GTPase Hbs1 (see Fig. 1a for human orthologs), which loads Dom34, a catalytically-inactive member of the archaeo-eukaryotic Release Factor 1 (aeRF1) superfamily. Hbs1•Dom34 and the ATPase Rli1 dissociate stalled ribosomes into 40S and 60S subunits. However, the 60S subunits retain the peptidyl-tRNA NCs, which recruit the ribosome quality control (RQC) complex comprised of Rqc1•Rqc2•Ltn1•Cdc48•Ufd1•Npl4. NCs ubiquitylated by the E3/ubiquitin ligase Ltn1 are extracted from the 60S by the ATPase Cdc48•Ufd1•Npl4 and presented to the 26S proteasome for degradation[3–9]. Failure to degrade the NCs leads to protein aggregation and proteotoxic stress in yeast and neurodegeneration in mice[10–14]. Despite intensive investigations on the RQC pathway, it is not known how the tRNA is hydrolyzed from the ubiquitylated NC prior to its degradation. Here we show that the Cdc48 adaptor Vms1 is a peptidyl-tRNA hydrolase. Similar to classical eRF1, Vms1 activity is dependent on a conserved catalytic glutamine. Evolutionary analysis indicates that yeast Vms1 is the

[*]**Corresponding Authors**. Correspondence to Aravind L (aravind@ncbi.nlm.nih.gov) and Raymond J. Deshaies (deshaies@caltech.edu).

Contributions.

R.V., K.R. and R.J.D. designed experiments, J.R. performed MS analyses, A.L. and A.M.B. did the computational analyses, K.R. performed the mutagenesis analyses, R.O. generated all the yeast strains and R.V. performed all the biochemical experiments. R.V. and R.J.D. supervised research, R.V., R.J.D. and A.L. wrote the paper and all authors participated in editing the manuscript. All figure schematics were generated by K.R.

Competing Financial Interests.

The authors (RV, KMR, AMB, RSO, JMR, AL) declare no competing financial interests. RJD is currently Senior Vice President of discovery research at Amgen and a Visiting Associate at the California Institute of Technology (Caltech).

Data Reporting. All data shown are representative of at least two independent biological experiments.

founding member of a clade of eRF1 homologs that we designate the Vms1-like RF1 clade (VLRF1).

Yeast Cdc48, a AAA+ ATPase that is conserved across eukaryotes and archaea, is a protein unfoldase[15,16] that engages in myriad cellular functions through binding of adaptors such as Ufd1•Npl4 (UN), which bind both Cdc48 and ubiquitylated substrate proteins. A protein A-based 'non-stop' substrate reporter (PrANS) encoded by an mRNA lacking a stop codon (Fig. 1b) accumulates on the ribosomal 60S subunit as a ubiquitylated species linked to tRNA when Cdc48 or UN function is compromised[7], suggesting that Cdc48•UN somehow extracts ubiquitylated NC from the 60S tunnel[6–8].

Two pieces of evidence implicated Vms1, which contains a Cdc48-binding VIM motif[17,18], in the RQC pathway. First, *vms1*Δ and RQC-deficient mutations cause a synthetic growth defect when combined with mutations that impair degradation of non-stop mRNA[8,19]. Second, *vms1*Δ[18] mutants, like *rqc2*Δ[20], are cycloheximide-sensitive. We extended this by showing that *vms1Δ*, like *ltn1*Δ and *cdc48*[7], displayed striking sensitivity to hygromycin, which binds the decoding center (Extended Data Fig. 1a).

To investigate further the role of Vms1 in degradation of non-stop proteins, we examined PrANS levels. PrANS conjugated to tRNA (PrANS-tRNA) accumulated in *vms1*Δ, but not in mutants lacking other Cdc48 adaptors (Fig. 1c). Additionally, *vms1*Δ accumulated high molecular weight (HMW) forms of PrANS. Treatment with RNase or deubiquitylase enzymes (Extended Data Fig. 1c) and pull-downs with ubiquitin-binding TUBE resin (Extended Data Fig. 1d) confirmed that HMW PrANS species were tRNA-linked ubiquitin conjugates (Ub-PrANS-tRNA).

Splitting of stalled 80S ribosomes is a prerequisite for stable association of Ltn1 with 60S subunits. Ltn1 then ubiquitylates the NCs prior to their degradation by 26S proteasomes[21]. To determine if Ub-PrANS-tRNA accumulated on 60S subunits in *vms1*Δ, we fractionated cell lysates on sucrose gradients. Immunoblotting for PrANS and the 60S protein Rpl3 revealed that Ub-PrANS-tRNA accumulated maximally in the first few Rpl3-containing fractions, which marks the position of 60S subunits (Fig. 1d)[7]. By contrast, non-ubiquitylated PrANS-tRNA that accumulated in both *vms1*Δ and *vms*Δ*ltn1*Δ cells was enriched on 80S subunits and polysomes. These data confirm that Ub-PrANS-tRNA accumulated on 60S subunits in *vms1*Δ in a manner that was dependent on Ltn1.

If Vms1 is directly involved in releasing stalled PrANS, it should bind ribosomes. To investigate this prediction, we immunoblotted sucrose gradient fractions from cells expressing Vms1 tagged with a triple HA epitope (Vms1^{HA3}). Whereas Ltn1 is restricted to 60S fractions[4], Vms1^{HA3} was detected across the entire gradient (Fig. 1e). This behavior suggests a broader function for Vms1 beyond its role in the RQC pathway. Interestingly, the 60S peak of Vms1^{HA3} was diminished and shifted towards lighter fractions in *ltn1*Δ cells (Fig. 1e), suggesting that in addition to Cdc48•UN[6], Ltn1 also promotes recruitment of Vms1 to 60S subunits. However, unlike Cdc48•UN, Vms1 was not identified as a component of RQC complex[6]. Consistent with this, Vms1 did not associate directly with UN (Extended Data Figs. 1e–h).

Given the exceptionally strong accumulation of PrANS-tRNA in *vms1*Δ, we wondered if Vms1 might have any relationship to known peptidyl-tRNA hydrolases. We carried out sensitive iterative sequence profile searches with PSI-BLAST and hidden Markov models seeded with the core RNaseH fold domain of the archaeal and eukaryotic RF1 proteins and the catalytically inactive Dom34 proteins, which are both members of the archaeo-eukaryotic RF1 (aeRF1) superfamily (see Methods). Strikingly, these searches recovered the central globular region of Vms1 orthologs. Reciprocal PSI-BLAST searches with this region recovered several members of the aeRF1 superfamily. This relationship was emphatically confirmed with a profile-profile comparison using the HHpred program with an alignment of the central conserved region of aeRF1 run against the PDB database, which significantly recovered 1DT9 (human eRF1; p-value=4×10^{-5}). This showed that the central domain of Vms1 had a putative catalytic loop bearing a conserved glutamine (Q) comparable to the classic active site of aeRF1s (Figs. 2a, b). An aeRF1-like architecture was observed in the recently reported crystal structure of the middle domain of Vms1, but the putative active site loop was not resolved[22]. The conserved glutamine in the eRF1 protein coordinates a water molecule in the A-site at the peptidyl transferase center (PTC). Nucleophilic attack of the peptidyl-tRNA in the P site by this water molecule releases the completed polypeptide chain[23,24]. In addition to the putative active site glutamine, Vms1 also contains conserved vicinal arginines in the α-helix immediately following the active site loop (Figs. 2a, b). Equivalent arginines in eRF1 have been implicated in stabilization of the active site loop[23], and stimulation of GTPase eRF3[25]. Based on this striking confluence of similarities we designated Vms1 as the founding member of the Vms1-Like Release Factor-1 (VLRF1) clade within the aeRF1 superfamily. In addition to the eukaryotic orthologs of Vms1 the VLRF1 clade also contains members from certain bacteria, predominantly bacteroidetes and more divergent versions in certain Archaea (Extended Data Figs. 2a, b).

To determine if Vms1 indeed is a novel peptidyl-tRNA hydrolase we generated two separate point mutations (Q295L, Q295P) of the predicted catalytic glutamine, which abrogate eRF1 function in budding yeast[23] and bacterial RFs[26], respectively. We also generated a putative active site deletion mutant (ΔAS). All mutant proteins were expressed normally and bound ribosomes (Fig. 3a). Whereas wild type Vms1^{HA3} rescued *vms1*Δ, cells expressing the point mutants accumulated PrANS-tRNA (Fig. 3a left panel), which sedimented with ribosomes (middle panel) and was conjugated to Ub (right panel). Sucrose gradient fractionation confirmed that Ub-PrANS-tRNA accumulated on 60S subunits in cells expressing Vms1^{HA3}-Q295L (Fig. 3b). Remarkably, the mutant protein strongly accumulated on 60S subunits, and was depleted from low MW fractions (Fig. 3c). Consistent with their biochemical defect, the *vms1-Q295L*, *-Q295P*, and -Δ*AS* mutants were exquisitely sensitive to hygromycin and cycloheximide (Fig. 3d). The point mutants thus phenocopy *vms1*Δ, both genetically and biochemically.

The putative catalytic region of Vms1 and other VLRF1 proteins is flanked by additional N- and C-terminal domains. The N-terminal C2H2-Zinc finger of Vms1 is specifically related to those of Rei1 and certain SBDS paralogs, which function at late steps in 60S subunit maturation[27]. This suggests that Vms1 might contact the ribosome with its Rei1-like Zn-finger domain (Fig. 2c). Meanwhile, the Vms1 C-terminal region is characterized by a run of 3 ankyrin repeats, a treble-clef fold Zn-binding domain (VTC; lost in fungi) and a VIM

motif that binds Cdc48[17,18] (Fig. 2c). To probe the role of these other sequence features, we generated mutants including 'DNKR' (lacking four Rei1-like Zn-finger residues predicted to interact with 60S; see legend for details), 'RR' (lacking the conserved vicinal arginines in the catalytic domain), and 'ΔVIM', and expressed the proteins in a *vms1*Δ strain. All mutant proteins were expressed comparably to wild type (Extended Data Fig. 3a). To assess the effects of the mutations we performed sucrose gradient fractionation of ribosomes. Compared to *vms1*Δ rescued by wildtype *VMS1*^{HA3}, all mutants accumulated Ub-PrANS-tRNA in 60S fractions (Extended Data Fig. 3c). The 'RR' mutant exhibited the strongest accumulation, as well as conspicuous spreading of Ub-PrANS-tRNA into the 80S peak, which was also observed with the ΔVIM mutant. Interestingly, the 'DNKR' mutant protein was shifted to lighter fractions, with depletion from monosome and polysome fractions, consistent with a role for the zinc finger in binding ribosomes (Extended Data Fig 3d). Notably, the cycloheximide sensitivity of the various mutants mimics the data obtained with the reporter, with the ΔAS and 'RR' mutants being most sensitive (Extended Data Fig. 3b).

To address conclusively the hypothesis that Vms1 is a novel peptidyl-tRNA hydrolase, we sought to reconstitute peptidyl-tRNA hydrolytic activity in vitro. Wildtype and ^{His6}Vms1-Q295L were expressed in bacteria and purified (Extended Data Fig. 4a). For substrate, we employed 60S fractions from *vms1*Δ cells expressing PrANS. ^{His6}Vms1 and substrate were mixed and following incubation, peptidyl-tRNA was precipitated using CTAB. ^{His6}Vms1 promoted release of both Ub-PrANS-tRNA and PrANS-tRNA species from 60S subunits (Fig. 4a). In sharp contrast, ^{His6}Vms1-Q295L was unable to release modified substrate. This assay was reproducible but required extensive manipulations that resulted in spontaneous hydrolysis of the substrate during its preparation. In addition, it was difficult to reliably quantify heterogeneous Ub conjugates by immunoblot. Therefore, we turned to in vitro translation in rabbit reticulocyte lysate, which has been used to reconstitute ubiquitylation of RQC substrates[9,21]. These earlier studies demonstrated that ubiquitylation of the NC is delayed ~15 minutes following translation. Because the Vms1-dependent reaction (Fig. 4a) did not display strong dependence on substrate ubiquitylation, we ran brief translation reactions with a non-stop template encoding ^{Flag}CRP with a 30 nucleotide polyA tail to generate stalled NCs that had not yet been ubiquitylated, which simplified quantification. The major translation product (Fig. 4b) was confirmed by CTAB precipitation and RNase treatment to be tRNA-conjugated ^{Flag}CRPNSK$_n$ (Extended Data Fig. 4b). Consistent with a prior report[9], the stalled ^{Flag}CRPNSKn-tRNA was associated maximally with 80S fractions (Extended Data Fig. 4c).

To assay for eRF1-like peptidyl-tRNA hydrolytic activity, wildtype or mutant ^{His6}Vms1 was incubated with [^{35}S]-labeled substrate for increasing time (Fig. 4b). De-acylation of ^{Flag}CRPNSKn-tRNA with concomitant formation of unmodified substrate was observed within three minutes (Figs. 4b, c) and at concentrations as low as 25 nM ^{His6}Vms1 (Fig. 4d, quantified in Extended Data Fig. 4d), whereas essentially no hydrolysis above background was observed with ^{His6}Vms1-Q295L. Since recombinant yeast Vms1 was functional in this heterologous system, we next tested Ankzf1, the human Vms1 ortholog. Purified Ankzf1 (Extended Data Fig. 4a) catalyzed deacylation, whereas the active site mutant Ankzf1-Q246L was inactive (Fig. 4e and Extended Data Fig. 4e).

Like *vms1*Δ, *cdc48* mutant cells accumulate Ub-PrANS-tRNA on 60S subunits[7]. This raises the question, what is the role of Cdc48 in hydrolysis of peptidyl-tRNA? We were unable to establish ATP-dependence for the *in vitro* deacylation reaction (not shown), which perhaps is not surprising because ATPase Rli1 accelerates NC release by eRF1 in the presence of non-hydrolyzable ATP[5]. We suggest that Cdc48 facilitates presentation of the catalytic glutamine of Vms1 at the PTC, much as Rli1 positions eRF1 in canonical termination[28]. A scaffolding function could account for accumulation of ubiquitylated reporter in 60S and 80S fractions in *vms1*-Δ*VIM* mutants (Extended Data Fig. 3c). Cdc48 ATPase working jointly with Ltn1 may play an additional role at the exit tunnel post-deacylation. The emerging NC is ubiquitylated by Ltn1 which recruits Cdc48•UN[6,7]. The latter can translocate along and unfold the NC[15,16] thereby ensuring its extraction from the 60S subunit. In other contexts, different factors may facilitate NC clearance. For example, defective ribosome-NC complexes targeted to mitochondria become stuck during import[29]. Vms1 promotes clearance of these stalls in a VIM-independent manner. Due to close apposition of the stalled ribosome-NC and mitochondrial translocon[29], neither Ltn1 nor Cdc48•UN should gain access to the deacylated NC to ensure its extraction. Vms1 also localizes to the ER and the RQC pathway can rescue NC stalled at the Sec61 translocon[30].

Three observations point to an additional role for Vms1 in release of stalled NC-tRNA from intact ribosomes, which is also likely to be Ltn1-independent: (i) Vms1 associates with all forms of ribosomes and this persists in *ltn1*Δ (Fig. 1e), (ii) *vms1* mutant cells exhibited strong accumulation of PrANS-tRNA in both monosome and polysome fractions (Figs. 1d and 3b), and (iii) Low doses (Fig. 4d) of Vms1 rapidly (Fig. 4b) deacylated 80S-associated peptidyl-tRNA; note however that NC-engaged 60S subunits can re-associate with free 40S subunits in vitro to generate 80S RNCs[21].

We suggest that in vivo, the “leading” stalled ribosome on non-stop poly (A) mRNA with the A site occupied could be the monosome substrate for Vms1 (see Extended Data Fig. 5 for model). Cleavage by an unidentified endonuclease generates ribosomes on truncated mRNA with empty A sites that are known to be rescued by Dom34•Hbs1•Rli1[1]. Jammed NC-tRNA on these split 60S subunits is ubiquitylated by Ltn1 and the tRNA linkage is hydrolyzed by Vms1. Our discovery of Vms1 as the founding member of the VLRF1 clade reveals that multiple different functional peptidyl-tRNA hydrolase release factors belonging to the aeRF1 superfamily coexist in eukaryotic cells. We posit that VLRF1 and Dom34 evolved to protect the translation apparatus from errors in transcription and post-transcriptional processing that generate defective mRNAs.

Methods

Yeast strains and culture conditions

All strains used in the current study are listed in Extended Data Table 1. They were derived from the W303 or S288C backgrounds and grown as described in Verma et al.[7]

Western Blot Analyses

Antibodies used were: Peroxidase Anti-Peroxidase Soluble Complex (PAP; used to detect Protein A, Sigma, # P1291). Anti-Flag M2 (Sigma # F-1804), anti-TAP (Thermo Fisher # CAB1001, and anti-HA 3F10 (Roche/Sigma # 12013819001). Anti-Rpl32 and Rpl3 were a gift from Jonathan Warner.

Ribosome isolation and sub-fractionation

Sucrose cushion method for isolation of ribosomes, binding of ribosomal preparations to TUBE-UBA resin, sucrose density gradient centrifugation, and CTAB precipitation of peptidyl-tRNA from sucrose gradient fractions were performed as described previously in Verma et al.[7] TUBE resin was from Boston Biochem, # AM-130. CTAB (Hexadecyltrimethyl-ammonium bromide) was from Sigma (# 52365).

Site-Directed Mutagenesis

All expression constructs for mutational analysis were generated using the Q5-Site-Directed Mutagenesis Kit (NEB #E00554S) following the manufacturer's manual. Primers were designed using the online tool NEBaseChanger (http://nebasechanger.neb.com). Mutations were confirmed by Sanger Sequencing. All plasmids are listed in Table 1.

Purification of ^{His6}Vms1 and ^{His6}Vms1-Q295L from bacteria

Wildtype and mutant Vms1 (Extended Data Table 1) were cloned into the bacterial pET-28a vector in frame with the N-terminal His6 tag. Expression was induced in Rosetta cells using 1mM IPTG at 16°C for 16 hours. Cell pellets were brought up in lysis buffer containing 50mM Hepes, pH 8.0, 0.5M NaCl, 20mM Imidazole and 0.5% Triton, sonicated, and centrifuged at 17,000 rpm for 20 min in a Sorvall SS34 rotor. Supernatant was bound to Ni-NTA affinity resin (Qiagen) for 1 hour at 4°C. Bound proteins were washed 4X in lysis buffer and eluted in 25mM Hepes, pH 7.5, 150mM NaCl, 5% glycerol and 250mM Imidazole. Imidazole was removed by dialysis and protein concentrated using Amicon Ultra centrifugal filters.

Purification of Ankzf1^{FlagMyc} and Ankzf1^{FlagMyc}-Q246L—Plasmids were constructed that contained the CMV promoter followed by sequences encoding wild type (Origene) or Q246L Ankzf1 (current study; confirmed by sequencing) tagged with a FlagMyc epitope at the 3' end of the open reading frame. These constructs were transiently transfected into human embryonic kidney HEK293 cells (ATCC, tested negative for mycoplasma contamination; DTC # 264). After 72 hours, proteins were purified by virtue of the Flag epitope using the protocol for Flag-tagged mammalian proteins reported by Shao et al.[21].

In vitro Transcription and Translation

PCR products were generated using 3XFlag-CRP (Extended Data Table 1) as template with reverse primer either containing a stop codon (3XFlag-CRPStop), or lacking a stop codon but with a 30 nucleotide polyT extension (3XFlag-CRPNSKn). PCR products were transcribed and translated in vitro using TnT T7 Quick rabbit reticulocyte lysate (Promega, #

L5540) in the presence of radioactive methionine (Perkin Elmer, #NEG709A). Reactions were typically for 30 mins at 30°C, at which time recombinant proteins were added for another 10 mins. Aliquots were resolved by SDS-PAGE, and dried gels were either exposed to film or to a PhosphorImager screen.

Isolation of TAP-tagged complexes from yeast

Cells in which *CDC48, VMS1*, or *UFD1* were tagged at the 3' end with the Tandem Affinity Purification (TAP) epitope[31] were grown to exponential phase in 2 L YPD medium and harvested. Washed cell pellets were ground in liquid nitrogen, and resuspended in 0.5× the volume of powder in a lysis buffer containing 25mM Tris, pH 7.5, 150mM NaCl, 0.25% Triton and protease inhibitor tablets (Roche, # 11873580001). Following centrifugation at 17000 rpm for 20 minutes (Sorvall SS34 rotor), lysates were bound to 200 ul acid-washed IgG sepharose 6 Fast Flow (GE Healthcare, # 17-0969-01) at 4°C for 90 mins. Bound proteins were washed 2× in lysis buffer, 2× in TEV buffer (25mM Tris, pH 7.5, 150 mM NaCl, 2mM DTT, 5% glycerol) and eluted by cleavage with 50 units TEV for 2 hours at 16°C.

Mass spectrometry analyses

Eluted samples were lyophilized and digested for mass spectrometry analysis as described in Pierce et al.[32] Approximately 250ng of trypsin-digested peptides were loaded onto a 26-cm analytical HPLC column (75 μm inner diameter) packed in-house with ReproSil-Pur C_{18AQ} 1.9-μm resin (120-Å pore size; Dr. Maisch, Ammerbuch, Germany). Once loaded, the peptides were separated with a 120-min gradient at a flow rate of 350 nl/min at 50°C (column heater) using the following gradient: 2–6% solvent B (7.5 min), 6–25% B (82.5 min), 25–40% B (30 min), 40–100% B (1 min), and 100% B (9 min), where solvent A was 97.8% H_2O, 2% ACN, and 0.2% formic acid, and solvent B was 19.8% H_2O, 80% ACN, and 0.2% formic acid. Samples were analyzed using an EASY-nLC 1000 coupled to an Orbitrap Fusion operated in data-dependent acquisition mode to automatically switch between a full scan (m/z = 350–1500) in the Orbitrap at 120,000 resolving power and an MS/MS scan of higher-energy collisional dissociation fragmentation detected in the ion trap (using TopSpeed). The automatic gain control (AGC) targets of the Orbitrap and ion trap were 400,000 and 10,000, respectively.

Mass Spec Data analysis

All raw data were searched concurrently using MaxQuant (version 1.5.3.30;[33,34]) against the Saccharomyces Genome Database (SGD) and a common contaminant database. Precursor mass tolerance was 4.5 ppm after automatic recalibration. Fragment ion tolerance was 0.5 Da. Searches permitted up to two missed tryptic peptide cleavages. Cysteine carbamidomethylation was designated as a fixed modification while Methionine oxidation and N-terminal acetylation were designated as variable modifications. iBAQ protein quantification and "match between runs" were enabled. Protein and peptide false discovery rates were estimated to be <1% using a target-decoy approach.

Computational Analyses

Iterative sequence profile searches were performed using the PSI-BLAST[35] and JACKHMMER[36] programs run against the NCBI non-redundant protein database (nr) clustered at 50% identity using the MMseqs2 program. Similarity-based clustering for both classification and culling of nearly identical sequences was performed using the BLASTCLUST program (ftp://ftp.ncbi.nih.gov/blast/documents/blastclust.html). The length (L) and score (S) threshold parameters were variably adjusted depending on need. For example, the length (L) and score (S) threshold parameters for clustering near identical proteins was L = 0.9 and S = 1.2. The HHpred program was used for profile-profile searches[37]. Structure similarity searches were performed using the DaliLite program[38]. Multiple sequence alignments were made using the Kalign program followed by manual adjustments on the basis of profile-profile and structural alignments[39]. Secondary structures were predicted using the JPred program[40]. For previously known domains, the Pfam database[41] was used as a guide, though the profiles were augmented by addition of newly detected divergent members that were not detected by the original Pfam models. Clustering with BLASTCLUST followed by multiple sequence alignment and further sequence profile searches were used to identify other domains that were not present in the Pfam database. Contextual information from prokaryotic gene neighborhoods was retrieved by a Perl script that extracts the upstream and downstream genes of the query gene and uses BLASTCLUST to cluster the proteins to identify conserved gene-neighborhoods. Phylogenetic analysis was conducted using an approximately-maximum-likelihood method implemented in the FastTree 2.1 program under default parameters[42]. Structural visualization and manipulations were performed using the PyMol 1.8.2.0 (Open Source; http://www.pymol.org) program.

Data Availability

Gel source images for Figs. 1, 3, 4 and Extended Data Figs. 1, 3 and 4 are available in Supplementary Fig. 1. Source data for quantifications in Figs. 4 and Extended Data Fig. 4 are provided in the online version of the paper. All other data supporting the findings of this study are available from the corresponding authors upon reasonable request.

Extended Data

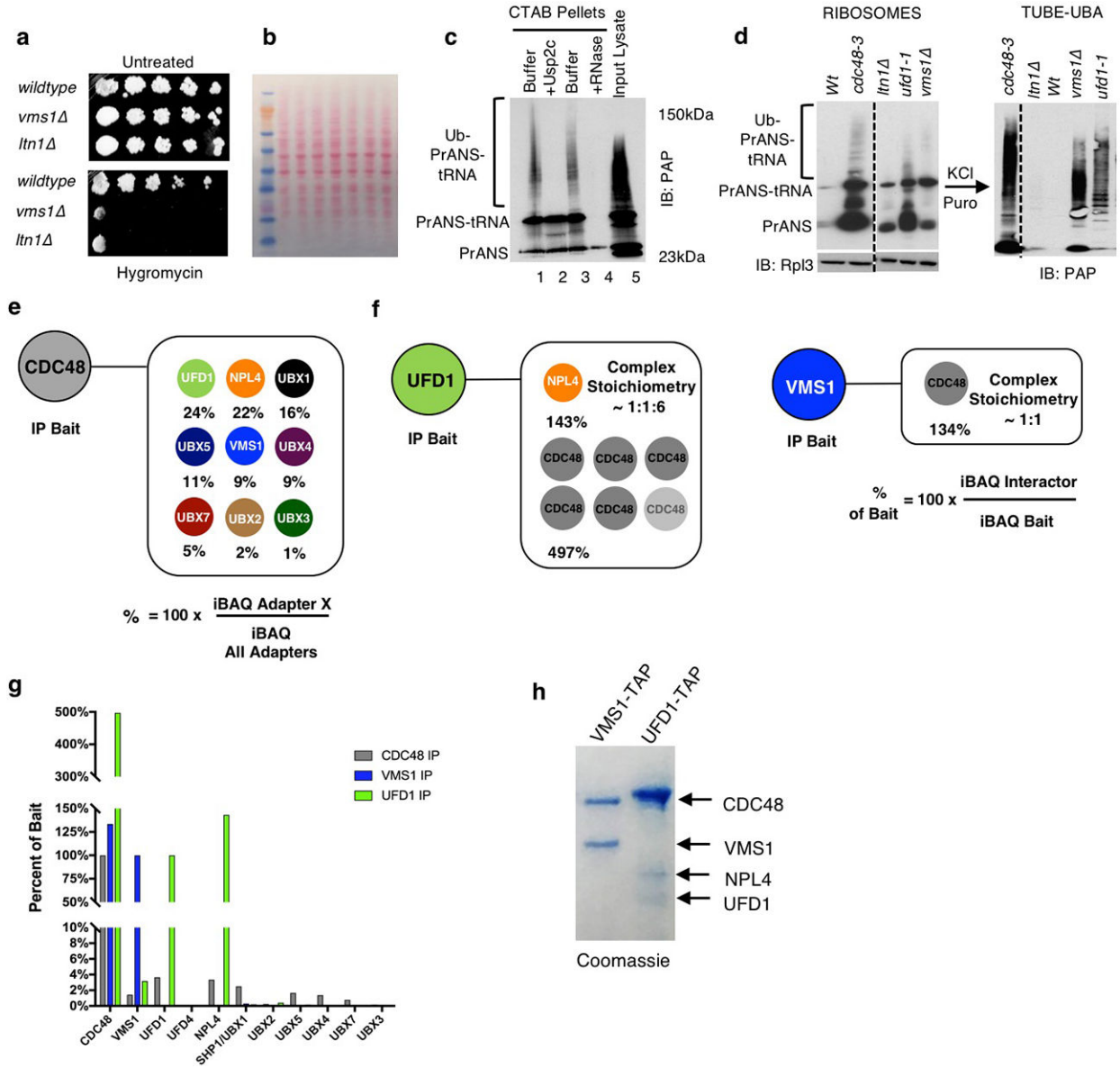

Extended Data Figure 1. Mass spectrometric analysis of Vms1 required for release of Ub-PrANS-tRNA from ribosomes

a, Serial 10-fold dilutions of exponential cultures were spotted on YPD plates with or without 100μg/ml Hygromycin B and allowed to grow at 30°C for 3 days. Data shown is representative of 3 biological replicates. **b**, Ponceau S stained nitrocellulose filter used as loading control for Fig. 1c. **c**, Lysate from *vms1Δ* cells expressing PrANS (Input, lane 5) was fractionated on a sucrose gradient and 60S fractions were pooled and mock-treated (lanes 1, 3) or pretreated with the deubiquitylating enzyme Usp2c (1μM; lane 2) or 100 μg/ml RNase A (lane 4) at 30°C for 20 minutes prior to CTAB precipitation. The pellets were IB with PAP. **d**, Ribosomes from the indicated strains were isolated using sucrose cushions and aliquots were IB to detect PrANS and Rpl3. The remainder was bound to

TUBE resin. The adsorbed fractions were IB with PAP. All lanes of the left and right panels are from the same blots. The dashed lines indicate cropping of lanes not pertinent to the current study. Gel source uncropped data are shown in Supplementary Fig.1. Data in **c** and **d** are representative of two biological replicates. **e–h**, Mass spectrometric analysis of TAP-tagged Cdc48, Vms1 and Ufd1. **e**, Relative abundance of each Cdc48 adapter co-immunoprecipitated with Cdc48 relative to all adapter proteins identified. **f,** Schematic illustrating the estimated stoichiometry of Cdc48●adapter complexes. **g**, Relative stoichiometry of associated proteins co-immunoprecipitated with Cdc48, Vms1 and Ufd1. Samples were normalized to the iBAQ value of the bait protein and presented as percent of bait protein. Protein iBAQ values from the untagged control was subtracted from the tagged immunoprecipitation samples. **h,** Coomassie blue stained gel of samples used for mass spec analysis. All mass spec data (e–h) are representative of two biological replicates.

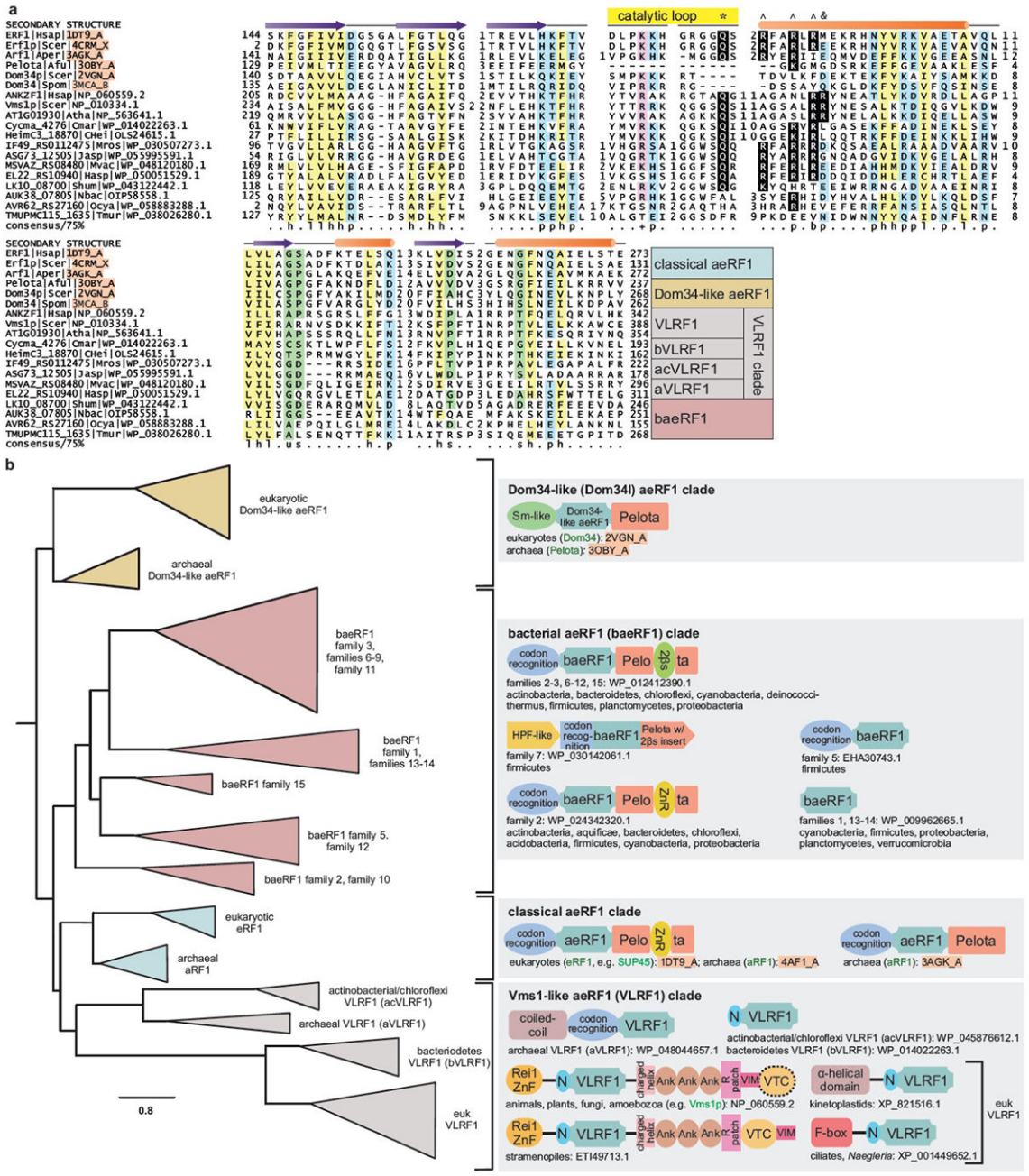

Extended Data Figure 2. Vms1 is the founding member of the VLRF1 clade

a, Extended sequence alignment of aeRF1 superfamily with representatives from all families/clades (compared to the limited subset in Fig. 2a). **b**, Phylogenetic tree depicting relationships within the aeRF1 superfamily; coloring matches clade labels in Fig. 2a. In the classical aeRF1 clade two branches respectively contain eukaryotic orthologs (eRF1) and archaeal orthologs (aRF1). Of the bacterial (baeRF1) versions, certain members are misannotated as “Host_attach” in the Pfam database while most cannot be detected by existing profiles. The total number of prokaryotic representatives of the VLRF1 clade in the non-redundant database (NCBI, Dec 1, 2017) is 1044. Of these the archaeal VLRF1 family

(aVLRF1) has 279, actino-chloroflexi VLRF1 family (acVLRF1) has 669 and the bacteroidetes VLRF1 family (bVLRF1) has 96 representatives. Notable domain architectures and conserved gene neighborhoods are shown to the right of tree. A gene encoding a ribosome hibernation factor (HPF1/YfiA) that facilitates inactive ribosome aggregation, frequently co-occurs and is predicted to function with the baeRF1 domains. Labels below name the well-characterized clade representatives, PDB structure IDs, and phyletic distributions. Dashed outline indicates domain is not universally present.

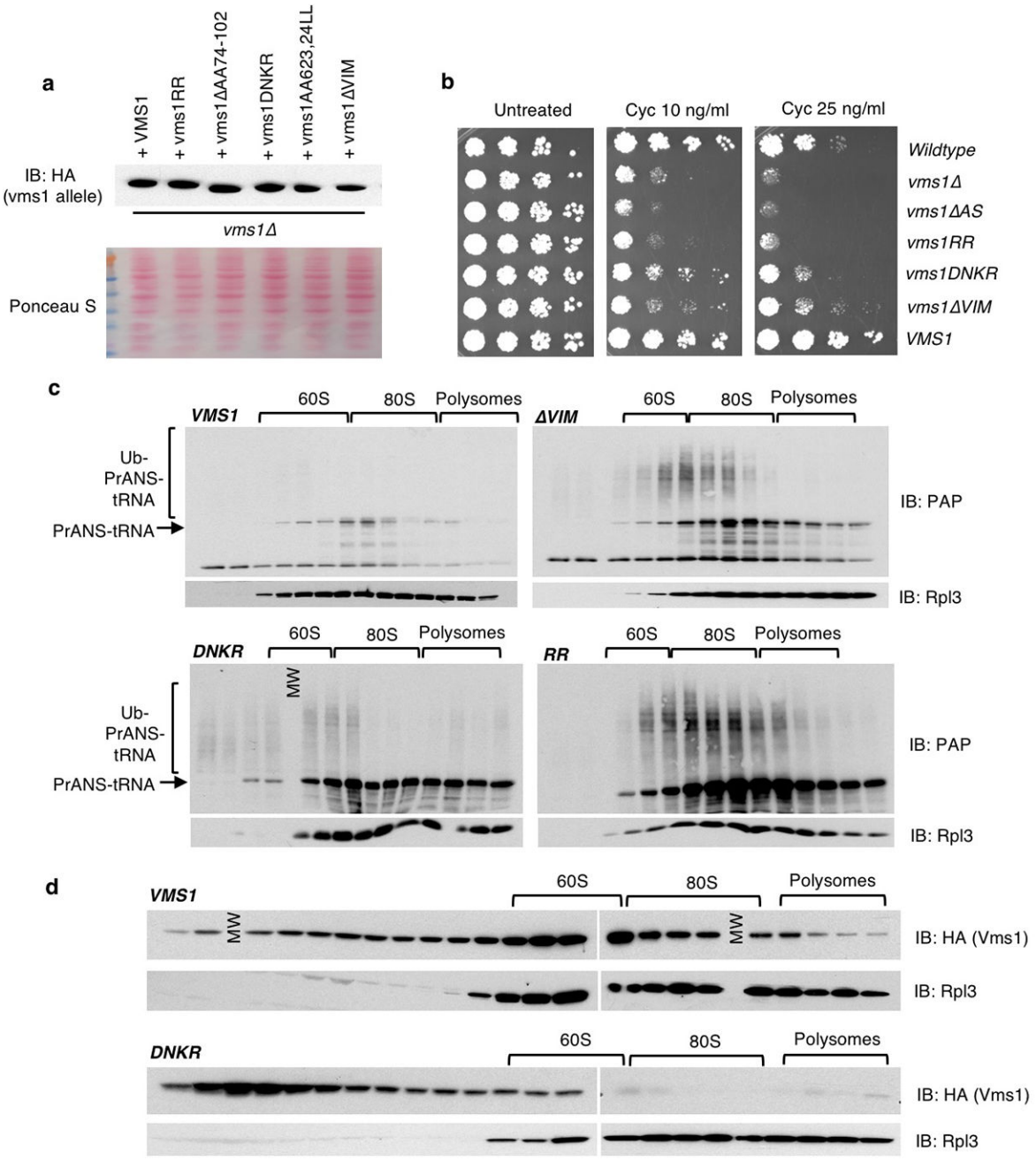

Extended Data Figure 3. Mutagenesis of the non-catalytic domains of Vms1

a, SDS lysates of the cells used in **c** below were IB with anti-HA. Ponceau S staining of blot shows equivalency of extracts. **b,** Serial 10 -fold dilutions of WT and *vms1Δ* cells transformed with the indicated *vms1* alleles were spotted on YPD plates containing 10 or 25 ng/ml cycloheximide and incubated at 30°C for 3 days. Data are representative of three biological replicates. **c**, Native lysates (10 A_{260} units each) were subjected to sucrose gradient analysis. In each case fractions 10–23 were resolved and IB to detect PrA and Rpl3. Identical exposures are shown for all panels. The RR mutant is R313AR314A. The DNKR mutant contains the following four mutations in the Zn-finger domain: D94A, N99A, K101A, and R102A. The ΔVIM mutant is deleted for amino acids 622–625. **d,** Native lysates of *vms1Δ* cells expressing wildtype $Vms1^{HA3}$ or $Vms1^{HA3}$-DNKR were subjected to sucrose gradient analysis. Fractions were IB for Vms1 and Rpl3. (MW: molecular weight standards). All Western blot data are representative of two biological replicates. Gel source data: Supplementary Fig. 1.

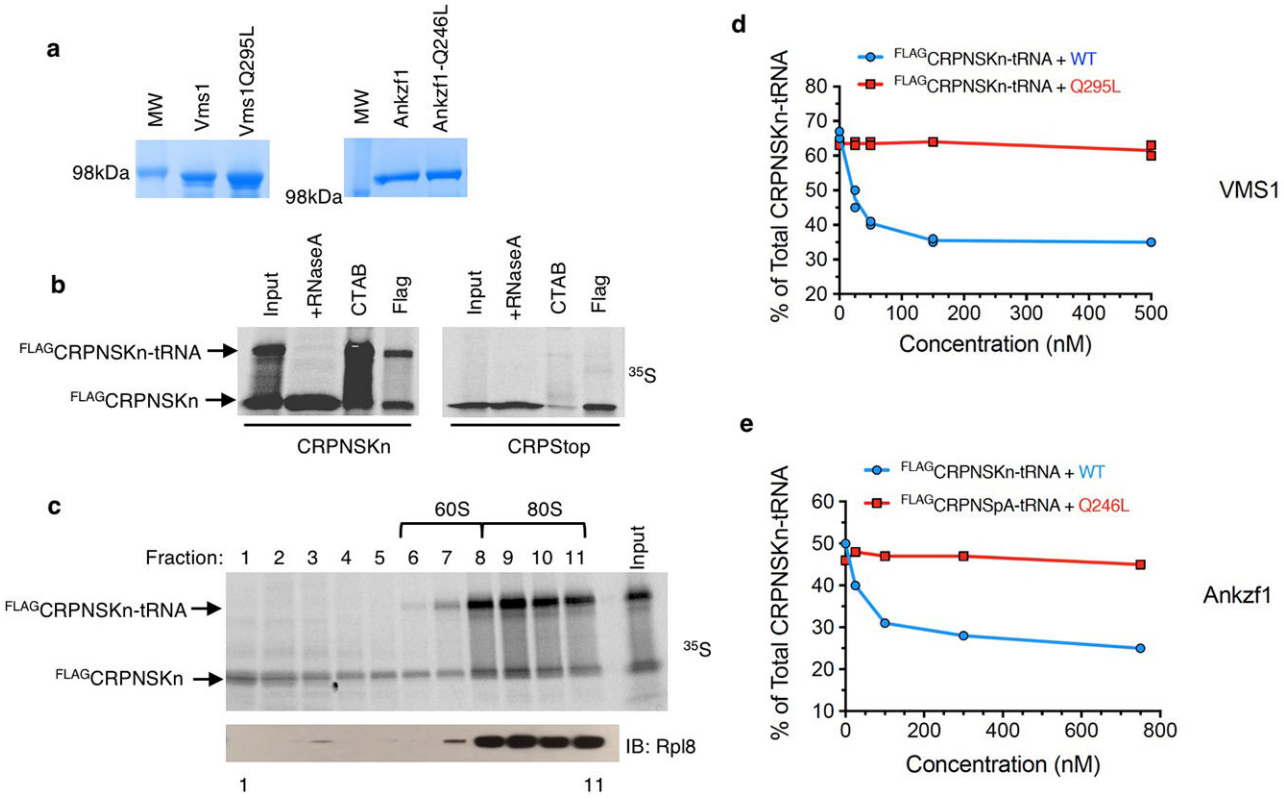

Extended Data Figure 4. In vitro reconstitution of Vms1 peptidyl-tRNA hydrolase activity

a, Coomassie Blue stained gels of indicated purified proteins used for in vitro reconstitution. **b**, Analysis of ribosome-nascent chain complexes generated by translation in reticulocyte lysate. PCR products encoding ^{FLAG}CRPNS followed by a 30 nucleotide polyA sequence and ^{FLAG}CRPStop (with a stop codon) were transcribed and translated in reticulocyte lysate in the presence of ^{35}S-methionine. Completed translation reactions were treated as described below, fractionated by SDS-PAGE, and visualized by autoradiography. Lane 1: no treatment; lane 2: +RNase A; lane 3: treated with CTAB; lane 4: immunoprecipitated with anti-FLAG resin. For lanes 3 and 4, the pellet fraction was analyzed. **c**, Sucrose gradient analysis of

reticulocyte translation reactions. ^{FLAG}CRPNSKn was transcribed and translated in 200 µl reticulocyte lysate. Following 30 mins of translation, lysates were layered onto 2 ml 10–50 % sucrose gradients and centrifuged using a Beckman SW55 rotor for 80 mins. 11 fractions (200 µl each) were collected from the top by hand. Aliquots were analyzed for fractionation of ^{35}S-labeled substrate and Rpl8 by autoradiography and IB, respectively. **d**, Quantification of two independent biological replicates of yeast ^{His6}Vms1 and ^{His6}Vms1-Q295L titration reactions shown in Fig. 4d. **e**, Quantification of titrations of human Ankzf1 and Ankzf1-Q246L shown in Fig. 4e. Representative of two biological replicates. All gel image and quantification source data in Supplementary Fig. 1.

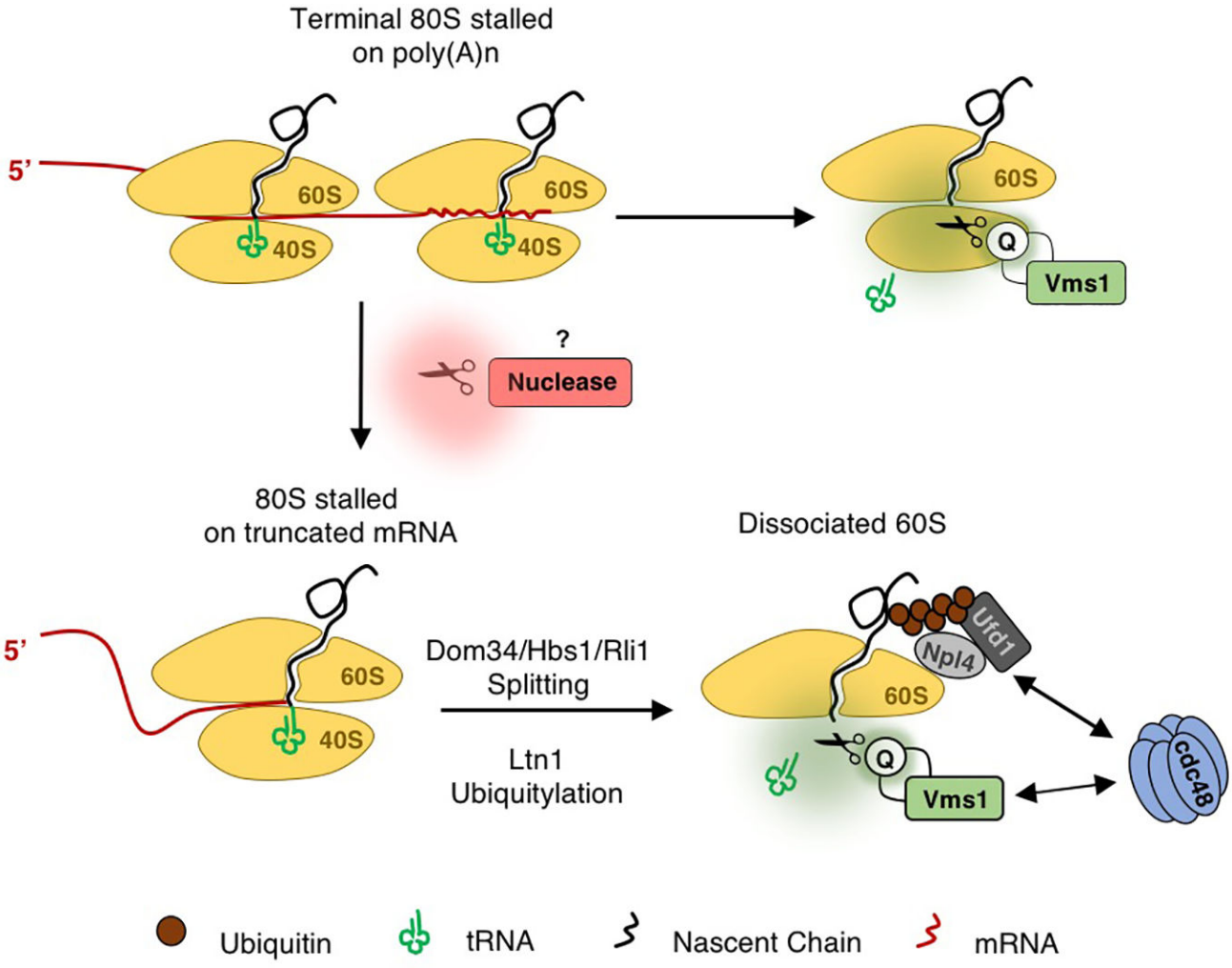

Extended Data Fig. 5. Working model of Vms1 function at stalled ribosomes

In non-stop decay of mRNAs lacking a stop codon, ribosomes translate the poly(A) tail and stall after translating several lysines[4,19]. The A site as a consequence is occupied by a AAA codon. Our data suggest that Vms1 can potentially hydrolyze peptidyl-tRNA chains on this leading stalled ribosome without prior splitting by Dom34•Hbs1•Rli1. One of the known responses to stalling is endonucleolytic cleavage of the mRNA by an as-yet unidentified endonuclease. The cleavage reaction generates a truncated transcript. Lagging ribosomes

that translate up to the cleavage site stall with an empty A site. Such stalls are recognized by Dom34•Hbs1 that together with Rli1 dissociate the 80S into 40S and 60S containing the nascent peptidyl-tRNA[1]. Dissociation allows for stable association of the RQC complex members Rqc1•Rqc2 and the E3 ubiquitin ligase Ltn1[9]. Rqc2 adds non-templated Ala and Thr residues to the C-terminal end of the NC to extrude sequences in the exit tunnel past the active site of Ltn1, which ubiquitylates Lys residues in the emerging nascent chain[10] and with the aid of Cdc48, optimizes the conformation of Vms1 at the PTC such that it can hydrolyze the tRNA. The ubiquitylated nascent chain is engaged by Ufd1/Npl4 bound to Cdc48 that together unfold and extract the NC. Dissociation of Rqc2 enables access of Vms1 to the 60S subunit[29], resulting in hydrolysis of the peptidyl-tRNA. Cdc48•Ufd1•Npl4 recruited to the ubiquitylated NC[7] ensures its efficient extraction from the 60S subunit. Regarding the action of Vms1 on 80S ribosomes, it is unclear if this activity is coupled in some manner to ribosome splitting.

Extended Data Table 1

Saccharomyces cerevisiae cell lines and Plasmids used.

RJD Number	Alias	Source	Genotype
6689	S288C	Open Biosystems	*his3Δ1, leu2Δ0, met15Δ0, ura3Δ0, a*
5970	S288C pProtein A Nonstop	This Study	*his3Δ1, leu2Δ0, met15Δ0, ura3Δ0, [pGAL-ProteinA-nonstop-PGK3'UTR-URA3]. a*
6646	ubx3 Δ pProtein A Nonstop	This Study	*his3Δ1, leu2Δ0, met15Δ0, ura3Δ0, ubx3::KANMX, [pGAL-ProteinA-Nonstop-PGK3'UTR-URA3], a*
6647	ubx4 Δ pProtein A Nonstop	This Study	*his3Δ1, leu2Δ0, met15Δ0, ura3Δ0, ubx4::KANMX, [pGAL-ProteinA-Nonstop-PGK3'UTR-URA3], a*
6648	ubx5Δ pProtein A Nonstop	This Study	*his3Δ1, leu2Δ0, met15Δ0, ura3Δ0, ubx5::KANMX, [pGAL-ProteinA-Nonstop-PGK3'UTR-URA3], a*
6654	ufd2Δ pProtein A Nonstop	This Study	*his3Δ1, leu2Δ0, met15Δ0, ura3Δ0, ufd2::KANMX, [pGAL-ProteinA-Nonstop-PGK3'UTR-URA3], a*
6651	ufd3Δ pProtein A Nonstop	This Study	*his3Δ1, leu2Δ0, met15Δ0, ura3Δ0, ufd3::KANMX, [pGAL-ProteinA-Nonstop-PGK3'UTR-URA3], a*
6640	vms1Δ pProtein A Nonstop	This Study	*his3Δ1, leu2Δ0, met15Δ0, ura3Δ0, vms1::KANMX, [pGAL-ProteinA-nonstop-PGK3'UTR-URA3], a*
5510	Itn1Δ pProtein A Nonstop	This Study	*his3Δ1, leu2Δ0, met15Δ0, ura3Δ0, Itn::KANMX, [pGAL-ProteinA-nonstop-PGK3'UTR-URA3], a*
6670	ufd1-1 pProtein A Nonstop	This Study	*his4-519, ura3-52, ade1-100, leu2-3, 112, ufd1-1, TRP+, pGAL-ProteinA-nonstop-PGK3'UTR-URA3]*
6722	Itn1Δ vms1Δ pProtein A Nonstop	This Study	*his3Δ1, leu2Δ0, met15Δ0, ura3Δ0, vms1::KANMX, Itn1::KANMX, [pGAL-ProteinA-nonstop-PGK3'UTR-URA3], a*
6771	vms1Δ Itn1Δ pVMS1-HA	This Study	*his3Δ1, leu2Δ0, met15Δ0, ura3Δ0, vms1::KANMX, Itn1::KANMX, [YCplac111-VMS1-3HA], a*

RJD Number	Alias	Source	Genotype
5445	vms1 Δ	Open Biosystems	*his3Δ1, leu2Δ0, met15Δ0, ura3Δ0, vms1::KANMX, a*
5400	Itn1Δ	Open Biosystems	*his3Δ1, leu2Δ0, met15Δ0, ura3Δ0, Itn1::KANMX, a*
6698	vms1Δ pVMS1 HA	This Study	*his3Δ1, leu2Δ0, met15Δ0, ura3Δ0, vms1::KANMX, [YCplac111-VMS1-3HA], a*
6732	vms1Δ pvms1 Q295L HA	This Study	*his3Δ1, leu2Δ0, met15Δ0, ura3Δ0, vms1::KANMX, [YCPlac111-vms1-Q295LΔ-3HA], a*
6701	vms1Δ pProtein A Nonstop VMS1-HA	This Study	*his3Δ1, leu2Δ0, met15Δ0, ura3Δ0, vms1::KANMX, [pGAL-ProteinA-nonstop-PGK3'UTR-URA3], [YCplac111-VMS1-3HA], a*
6705	vms1Δ pProtein A Nonstop vms1-Q295L-3HA	This Study	*his3Δ1, leu2Δ0, met15Δ0, ura3Δ0, vms1::KANMX, [pGAL-ProteinA-nonstop-PGK3'UTR-URA3], [YCplac111-vms1-Q295L-3HA], a*
6733	vms1Δ pvms1 Q295P	This Study	*his3Δ1, leu2Δ0, met15Δ0, ura3Δ0, vms1::KANMX, [YCPlac111-vms1-Q295PΔ-3HA], a*
6731	vms1Δ pVMS1 ASΔ 3HA	This Study	*his3Δ1, leu2Δ0, met15Δ0, ura3Δ0, vms1::KANMX, [YCPlac111-vms1-ActiveSiteΔ-3HA], a*
6740	vms1Δ pvms1 Δ622-625 (vimΔ) 3HA	This Study	*his3Δ1, leu2Δ0, met15Δ0, ura3Δ0, vms1::KANMX, [YCplac111-vms1-Δ622-625-3HA], a*
6739	vms1Δ pvms1 ΔIntR 3HA	This Study	*his3Δ1, leu2Δ0, met15Δ0, ura3Δ0, vms1::KANMX, [YCplac111-vms1-ΔIntR-3HA], a*
6738	vms1Δ pvms1RR3 13/314AA	This Study	*his3Δ1, leu2Δ0, met15Δ0, ura3Δ0, vms1::KANMX, [YCplac111-vms1-RR313/314-3HA], a*
6707	vms1Δ pProtein A Nonstop pvms1 ASΔ 3HA	This Study	*his3Δ1, leu2Δ0, met15Δ0, ura3Δ0, vms1::KANMX, [pGAL-ProteinA-nonstop-PGK3'UTR-URA3], [YCplac111-vms1-ASΔ-3HA], a*
6706	vms1Δ pProtein A Nonstop pvms1-Q295P-3HA	This Study	*his3Δ1, leu2Δ0, met15Δ0, ura3Δ0, vins1::KANMX, [pGAL-ProteinA-nonstop-PGK3'UTR-URA3], [YCplac111-vms1-Q295P-3HA], a*

Plasmid	Relevant Vector	Source
RDB2764	pGAL-ProteinA-nonstop-PGK3'UTR[URA3]	Ambro Van Hoof
RDB3226	YCplac111-VMS1-3HA	Alexander Buchberger
RDB3293	YCplac111-vms1 ΔAA74-102-HA	This Study
RDB3295	YCplac111-vms1 Δlnt R-HA	This Study
RDB3286	YCplac111-vms1 ASΔ-HA	This Study
RDB3287	Ycplac-111-vms1 Q295L-HA	This Study
RDB3288	YCplac111-vms1 Q295P-HA	This Study
RDB3292	YCplac111-vms1 RR3 13/3 14AA	This Study
RDB2632	pET28a-VMS1	Hai Rao
RDB3336	pET28a-vms1 Q295L	This Study
RDB3353	pCMV6-ANKZF1-mycDDK	Origene
RDB3359	pCMV6-ankzf1 Q246L-mycDDK	This Study

Plasmid	Relevant Vector	Source
RDB3299	T7-3xFLAG-CRP	This Study

Upper Table: List of yeast strains used in this study.
Lower Table: Plasmids used in this study.

Supplementary Material

Refer to Web version on PubMed Central for supplementary material.

Acknowledgments

We thank Drs. A. Buchberger, H. Rao, A. van Hoof, R. Voorhees and J. Warner for reagents. We thank the Proteome Exploration Laboratory (PEL), Caltech for help with the mass spectrometry analysis. We thank members of the Deshaies Lab, M. Blanco, M. Guttman, B. Clemons, R. Voorhees and S. Shan for fruitful discussions. RJD was an Investigator of the HHMI and this work was funded in part by HHMI. A.M.B and L.A are supported by the funds of the Intramural Research Program of the National Library of Medicine.

References

1. Buskirk AR, Green R. Ribosome pausing, arrest and rescue in bacteria and eukaryotes. Philos Trans R Soc Lond B Biol Sci. 2017; 372
2. Joazeiro CAP. Ribosomal Stalling During Translation: Providing Substrates for Ribosome-Associated Protein Quality Control. Annu Rev Cell Dev Biol. 2017
3. Ito-Harashima S, Kuroha K, Tatematsu T, Inada T. Translation of the poly(A) tail plays crucial roles in nonstop mRNA surveillance via translation repression and protein destabilization by proteasome in yeast. Genes Dev. 2007; 21:519–524. DOI: 10.1101/gad.1490207 [PubMed: 17344413]
4. Bengtson MH, Joazeiro CA. Role of a ribosome-associated E3 ubiquitin ligase in protein quality control. Nature. 2010; 467:470–473. DOI: 10.1038/nature09371 [PubMed: 20835226]
5. Shoemaker CJ, Green R. Kinetic analysis reveals the ordered coupling of translation termination and ribosome recycling in yeast. Proc Natl Acad Sci U S A. 2011; 108:E1392–1398. DOI: 10.1073/pnas.1113956108 [PubMed: 22143755]
6. Brandman O, et al. A ribosome-bound quality control complex triggers degradation of nascent peptides and signals translation stress. Cell. 2012; 151:1042–1054. DOI: 10.1016/j.cell.2012.10.044 [PubMed: 23178123]
7. Verma R, Oania RS, Kolawa NJ, Deshaies RJ. Cdc48/p97 promotes degradation of aberrant nascent polypeptides bound to the ribosome. Elife. 2013; 2:e00308. [PubMed: 23358411]
8. Defenouillere Q, et al. Cdc48-associated complex bound to 60S particles is required for the clearance of aberrant translation products. Proc Natl Acad Sci U S A. 2013; 110:5046–5051. DOI: 10.1073/pnas.1221724110 [PubMed: 23479637]
9. Shao S, von der Malsburg K, Hegde RS. Listerin-dependent nascent protein ubiquitination relies on ribosome subunit dissociation. Mol Cell. 2013; 50:637–648. DOI: 10.1016/j.molcel.2013.04.015 [PubMed: 23685075]
10. Shen PS, et al. Protein synthesis. Rqc2p and 60S ribosomal subunits mediate mRNA-independent elongation of nascent chains. Science. 2015; 347:75–78. DOI: 10.1126/science.1259724 [PubMed: 25554787]
11. Chu J, et al. A mouse forward genetics screen identifies LISTERIN as an E3 ubiquitin ligase involved in neurodegeneration. Proc Natl Acad Sci U S A. 2009; 106:2097–2103. DOI: 10.1073/pnas.0812819106 [PubMed: 19196968]
12. Choe YJ, et al. Failure of RQC machinery causes protein aggregation and proteotoxic stress. Nature. 2016; 531:191–195. DOI: 10.1038/nature16973 [PubMed: 26934223]
13. Yonashiro R, et al. The Rqc2/Tae2 subunit of the ribosome-associated quality control (RQC) complex marks ribosome-stalled nascent polypeptide chains for aggregation. Elife. 2016; 5:e11794. [PubMed: 26943317]

14. Defenouillere Q, et al. Rqc1 and Ltn1 Prevent C-terminal Alanine-Threonine Tail (CAT-tail)-induced Protein Aggregation by Efficient Recruitment of Cdc48 on Stalled 60S Subunits. J Biol Chem. 2016; 291:12245–12253. DOI: 10.1074/jbc.M116.722264 [PubMed: 27129255]
15. Blythe EE, Olson KC, Chau V, Deshaies RJ. Ubiquitin- and ATP-dependent unfoldase activity of P97/VCP*NPLOC4*UFD1L is enhanced by a mutation that causes multisystem proteinopathy. Proc Natl Acad Sci U S A. 2017; 114:E4380–E4388. DOI: 10.1073/pnas.1706205114 [PubMed: 28512218]
16. Bodnar NO, Rapoport TA. Molecular Mechanism of Substrate Processing by the Cdc48 ATPase Complex. Cell. 2017; 169:722–735. e729. DOI: 10.1016/j.cell.2017.04.020 [PubMed: 28475898]
17. Hanzelmann P, Schindelin H. The structural and functional basis of the p97/valosin-containing protein (VCP)-interacting motif (VIM): mutually exclusive binding of cofactors to the N-terminal domain of p97. J Biol Chem. 2011; 286:38679–38690. DOI: 10.1074/jbc.M111.274506 [PubMed: 21914798]
18. Stapf C, Cartwright E, Bycroft M, Hofmann K, Buchberger A. The general definition of the p97/valosin-containing protein (VCP)-interacting motif (VIM) delineates a new family of p97 cofactors. J Biol Chem. 2011; 286:38670–38678. DOI: 10.1074/jbc.M111.274472 [PubMed: 21896481]
19. van Hoof A, Frischmeyer PA, Dietz HC, Parker R. Exosome-mediated recognition and degradation of mRNAs lacking a termination codon. Science. 2002; 295:2262–2264. DOI: 10.1126/science.1067272 [PubMed: 11910110]
20. Alamgir M, Erukova V, Jessulat M, Azizi A, Golshani A. Chemical-genetic profile analysis of five inhibitory compounds in yeast. BMC Chem Biol. 2010; 10:6. [PubMed: 20691087]
21. Shao S, Hegde RS. Reconstitution of a minimal ribosome-associated ubiquitination pathway with purified factors. Mol Cell. 2014; 55:880–890. DOI: 10.1016/j.molcel.2014.07.006 [PubMed: 25132172]
22. Nielson JR, et al. Sterol Oxidation Mediates Stress-Responsive Vms1 Translocation to Mitochondria. Mol Cell. 2017; 68:673–685. e676. DOI: 10.1016/j.molcel.2017.10.022 [PubMed: 29149595]
23. Song H, et al. The crystal structure of human eukaryotic release factor eRF1--mechanism of stop codon recognition and peptidyl-tRNA hydrolysis. Cell. 2000; 100:311–321. [PubMed: 10676813]
24. Jin H, Kelley AC, Loakes D, Ramakrishnan V. Structure of the 70S ribosome bound to release factor 2 and a substrate analog provides insights into catalysis of peptide release. Proc Natl Acad Sci U S A. 2010; 107:8593–8598. DOI: 10.1073/pnas.1003995107 [PubMed: 20421507]
25. Cheng Z, et al. Structural insights into eRF3 and stop codon recognition by eRF1. Genes Dev. 2009; 23:1106–1118. DOI: 10.1101/gad.1770109 [PubMed: 19417105]
26. Korostelev A, et al. Crystal structure of a translation termination complex formed with release factor RF2. Proc Natl Acad Sci U S A. 2008; 105:19684–19689. DOI: 10.1073/pnas.0810953105 [PubMed: 19064930]
27. Greber BJ, et al. Insertion of the Biogenesis Factor Rei1 Probes the Ribosomal Tunnel during 60S Maturation. Cell. 2016; 164:91–102. DOI: 10.1016/j.cell.2015.11.027 [PubMed: 26709046]
28. Preis A, et al. Cryoelectron microscopic structures of eukaryotic translation termination complexes containing eRF1-eRF3 or eRF1-ABCE1. Cell Rep. 2014; 8:59–65. DOI: 10.1016/j.celrep.2014.04.058 [PubMed: 25001285]
29. Izawa T, Park SH, Zhao L, Hartl FU, Neupert W. Cytosolic Protein Vms1 Links Ribosome Quality Control to Mitochondrial and Cellular Homeostasis. Cell. 2017
30. von der Malsburg K, Shao S, Hegde RS. The ribosome quality control pathway can access nascent polypeptides stalled at the Sec61 translocon. Mol Biol Cell. 2015; 26:2168–2180. DOI: 10.1091/mbc.E15-01-0040 [PubMed: 25877867]
31. Puig O, et al. The tandem affinity purification (TAP) method: a general procedure of protein complex purification. Methods. 2001; 24:218–229. DOI: 10.1006/meth.2001.1183 [PubMed: 11403571]
32. Pierce NW, et al. Cand1 promotes assembly of new SCF complexes through dynamic exchange of F box proteins. Cell. 2013; 153:206–215. DOI: 10.1016/j.cell.2013.02.024 [PubMed: 23453757]

33. Cox J, Mann M. MaxQuant enables high peptide identification rates, individualized p.p.b.-range mass accuracies and proteome-wide protein quantification. Nat Biotechnol. 2008; 26:1367–1372. DOI: 10.1038/nbt.1511 [PubMed: 19029910]

34. Wagner SA, et al. A proteome-wide, quantitative survey of in vivo ubiquitylation sites reveals widespread regulatory roles. Mol Cell Proteomics. 2011; 10 M111 013284.

35. Altschul SF, et al. Gapped BLAST and PSI-BLAST: a new generation of protein database search programs. Nucleic Acids Res. 1997; 25:3389–3402. [PubMed: 9254694]

36. Eddy SR. A new generation of homology search tools based on probabilistic inference. Genome Inform. 2009; 23:205–211. [PubMed: 20180275]

37. Alva V, Nam SZ, Soding J, Lupas AN. The MPI bioinformatics Toolkit as an integrative platform for advanced protein sequence and structure analysis. Nucleic Acids Res. 2016; 44:W410–415. DOI: 10.1093/nar/gkw348 [PubMed: 27131380]

38. Holm L, Kaariainen S, Rosenstrom P, Schenkel A. Searching protein structure databases with DaliLite v.3. Bioinformatics. 2008; 24:2780–2781. DOI: 10.1093/bioinformatics/btn507 [PubMed: 18818215]

39. Lassmann T, Frings O, Sonnhammer EL. Kalign2: high-performance multiple alignment of protein and nucleotide sequences allowing external features. Nucleic Acids Res. 2009; 37:858–865. DOI: 10.1093/nar/gkn1006 [PubMed: 19103665]

40. Cole C, Barber JD, Barton GJ. The Jpred 3 secondary structure prediction server. Nucleic Acids Res. 2008; 36:W197–201. DOI: 10.1093/nar/gkn238 [PubMed: 18463136]

41. Finn RD, et al. The Pfam protein families database: towards a more sustainable future. Nucleic Acids Res. 2016; 44:D279–285. DOI: 10.1093/nar/gkv1344 [PubMed: 26673716]

42. Price MN, Dehal PS, Arkin AP. FastTree 2--approximately maximum-likelihood trees for large alignments. PLoS One. 2010; 5:e9490. [PubMed: 20224823]

a **Primary components of the yeast and mammalian ribosome quality control (RQC) pathway**

	Ribosome Splitting			Nascent-Chain Ubiquitylation			Nascent-Chain Extraction			Peptidyl-tRNA Hydrolase
Yeast	Hbs1	Dom34	Rli1	Rqc1	Rqc2	Ltn1	Cdc48	Ufd1	Npl4	Vms1
Mammals	HBS1L	Pelota	ABCE1	TCF25	NEMF	Listerin	VCP/p97	UFD1L	NPLOC4	Ankzf1

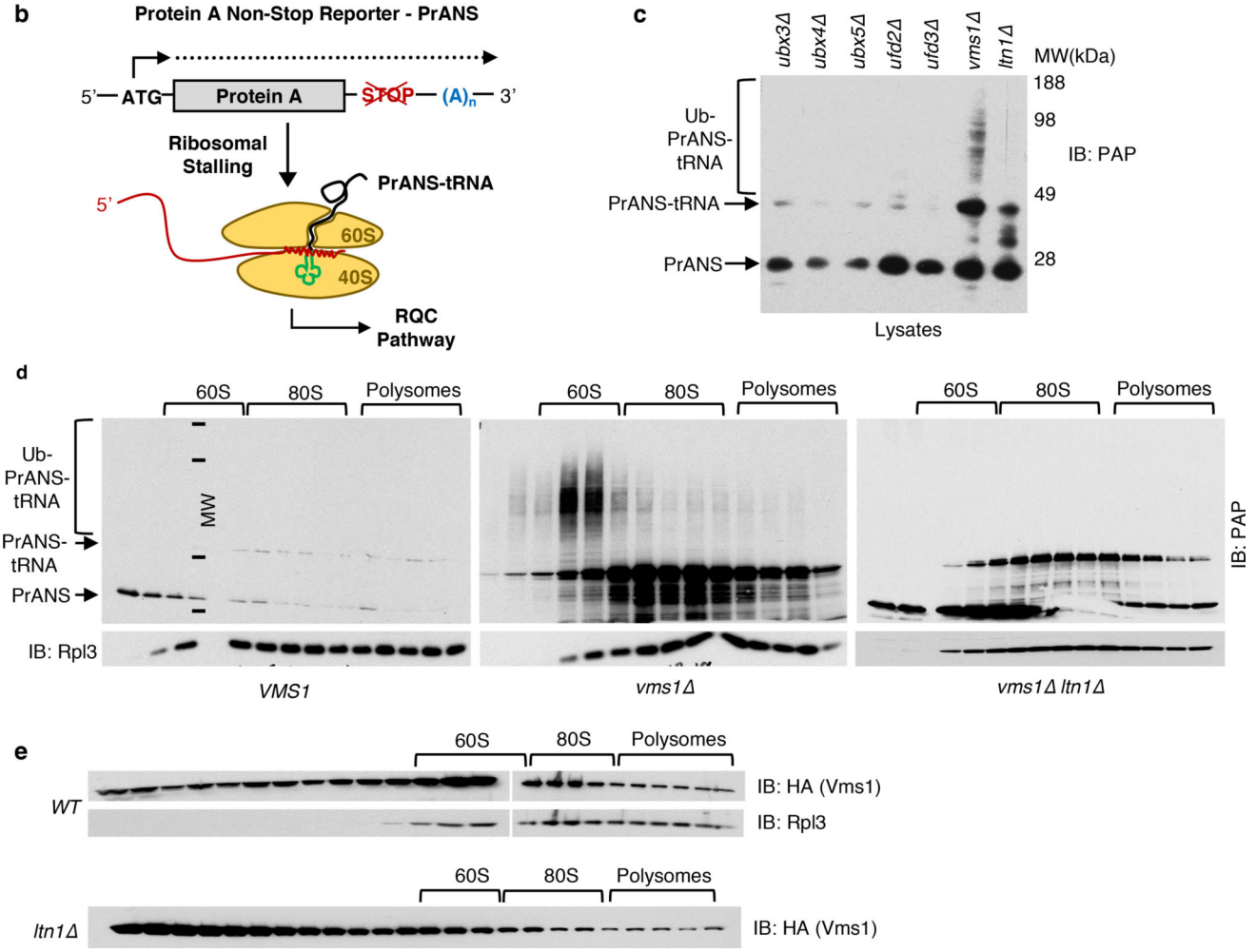

Figure 1. Vms1 is required for release of ubiquitylated, tRNA-linked non-stop protein A reporter (Ub-PrANS-tRNA) from 60S ribosomal subunits

a, Mammalian orthologs of the yeast RQC pathway. **b**, Model substrate reporter used to study the non-stop pathway. **c**, Mutants were lysed in denaturing SDS, fractionated on a NuPAGE gel, and immunoblotted (IB) with PAP to detect PrA. **d**, Native lysates (10 A_{260} units) were separated on sucrose gradients and fractions were resolved on TG gels and IB with PAP and anti-Rpl3. (MW: molecular weights 250, 150, 50, and 23 kDa indicated by marks). **e**, Native lysates from wild type (*WT*: *LTN1*) and *ltn1*Δ mutant cells expressing $Vms1^{HA3}$ were fractionated on sucrose gradients and IB with anti-HA and Rpl3. All Western blots are representative of two biological replicates. Gel source data: Supplementary Fig. 1.

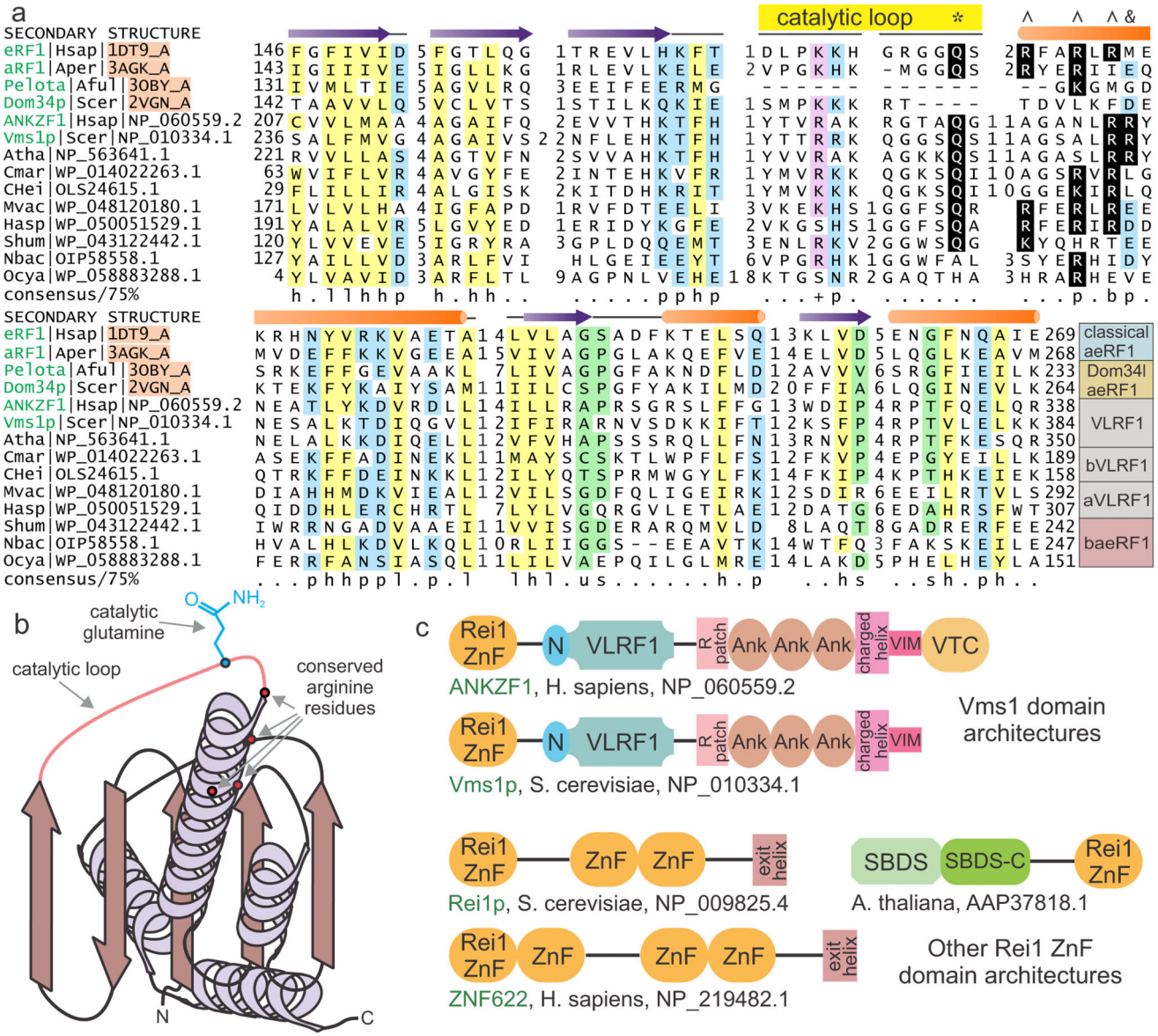

Figure 2. Vms1 is a member of the aeRF1 superfamily and the founding member of the VLRF1 clade

a, Multiple sequence alignment of the aeRF1 superfamily; families indicated on the right with accession numbers, organism abbreviations, and gene names on the left. Residues colored per consensus conservation, key residues and features marked at top ('*': catalytic glutamine, '^': arginine residues conserved across multiple families, "&": arginine conserved in VLRF1 family). **b**, Topology diagram of aeRF1 RNase H fold domain, key features labeled. **c**, Domain architectures of proteins containing the Rei1 C2H2-Zinc finger.

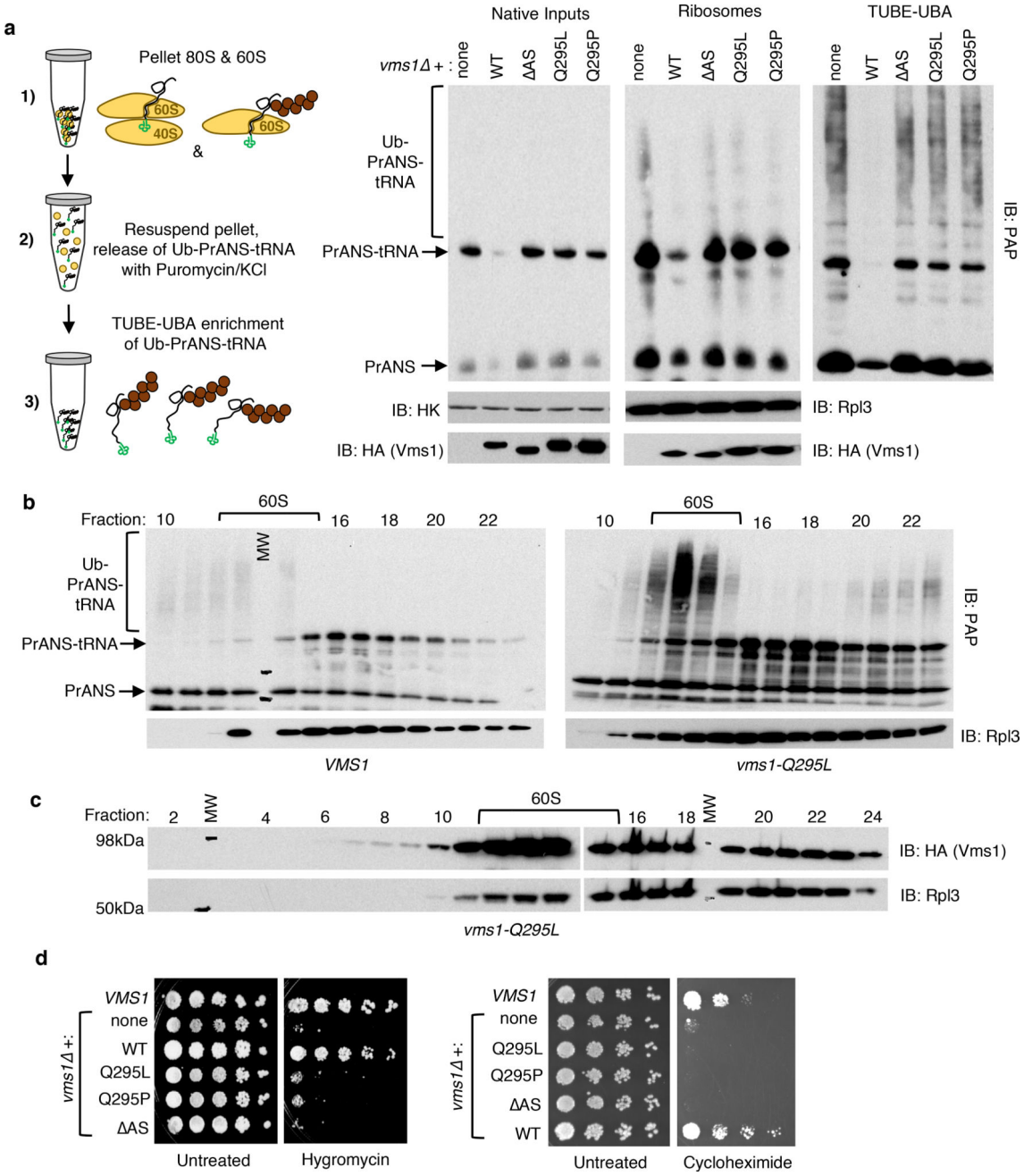

Figure 3. Point mutations in the conserved, putative peptidyl-tRNA hydrolase active site of Vms1 phenocopy *vms1Δ*

a, Schematic of experimental design. Brown circles: Ub, green: tRNA. Left panel: lysates from *vms1Δ* cells expressing either WT Vms1^{HA3} or the active site mutants were fractionated on a NuPAGE gel, and IB to detect PrA and Vms1^{HA3}. Hexokinase (HK) served as loading control. ΔAS lacks amino acids 283–314. Ribosomes (middle panel) were isolated on sucrose cushions, and aliquots IB to detect PrA, Rpl3, and Vms1^{HA3}. Right panel: the remaining ribosomes were adsorbed to TUBE resin and bound fractions were resolved by TG gels and IB to detect PrA. **b**, Native lysates (10 A_{260}) from *vms1Δ* expressing PrANS and either WT Vms1^{HA3} (left panel) or the Q295L mutant (right panel)

were fractionated on sucrose gradients and IB to detect PrA and Rpl3. (MW: 36 and 23kDa). **c,** Sucrose gradient fractions from *vms1Δ* expressing Vms1-Q295L^{HA3} were IB to detect mutant Vms1 and Rpl3. They were run at the same time as WT Vms1^{HA3} in Fig. 1e and the exposures are identical. **d,** Serial 10-fold dilutions of WT and *vms1Δ* cells transformed with the indicated *vms1* alleles were spotted on YPD plates containing 100μg/ml hygromycin or 25 ng/ml cycloheximide and incubated at 30°C for 3 days. A representative of three biological replicates is shown. All Western blots are representative of two biological replicates. Gel source data: Supplementary Fig. 1.

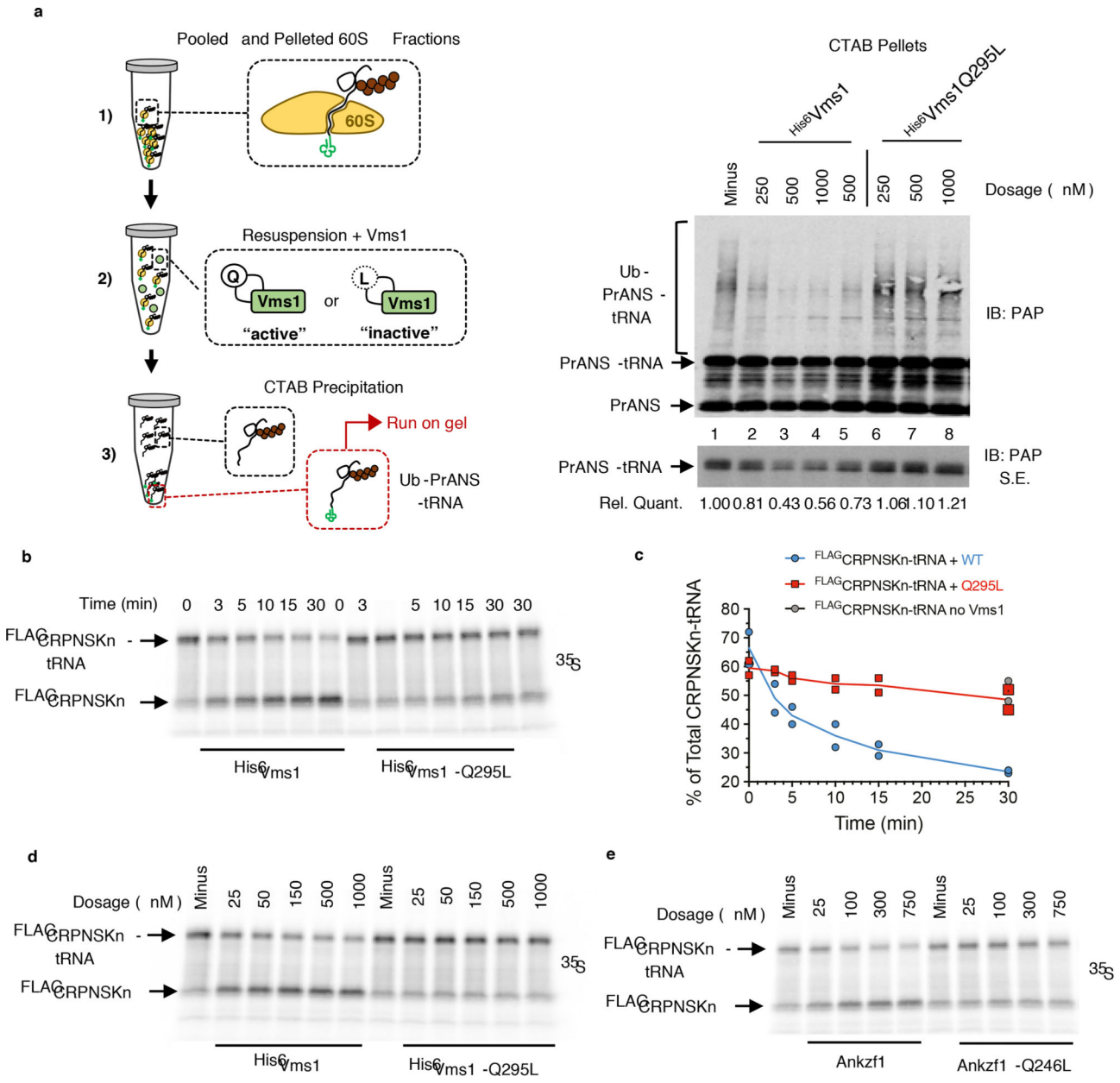

Figure 4. Peptidyl-tRNA hydrolase activity of Vms1 and Ankzf1 depend on the catalytic glutamine residue

a, Experimental design on left. Brown circles: Ub, green: tRNA. Lysate from *vms1Δ* cells expressing PrANS was fractionated on a sucrose gradient, and 60S fractions were pooled and pelleted.. ^{His6}Vms1 or ^{His6}Vms1-Q295L were added and incubated for 10 mins at 30°C. Ub-PrANS-tRNA was precipitated with CTAB, and IB with PAP to detect PrA. Bottom panel is shorter exposure (S.E.) of top from which the discrete peptidyl-tRNA band was quantified (Lane 5 contained additional 1mM GTP). Western blot is representative of two biological replicates. **b**, Time course of deacylation reaction using ribosome–NC complexes (RNCs) generated by in vitro translation. ^{Flag}CRPNSKn was translated in reticulocyte lysate in the presence of ^{35}S methionine for 30 minutes at 30°C. Recombinant WT or mutant

^{His6}Vms1 (150 nM) was added for the indicated time periods to RNCs (75–100 nM). Aliquots were visualized by autoradiography. **c,** Phosphorimager quantification of two independent biological replicates from b. WT: ^{His6}Vms1. Q295L: mutant ^{His6}Vms1. **d,** Titration of Vms1. Reactions and processing as in b. **e,** WT and mutant hAnkzf1 were analyzed as described in b, except that the hydrolase reaction was performed at 37°C. A representative of two biological replicates is shown. Gel source image data: Supplementary Fig. 1.